Temperature dependent electronic transport in concentrated solid solutions of the 3d-transition metals Ni, Fe, Co and Cr from first principles

G. D. Samolyuk, S. Mu, A. F. May, B. C. Sales, S. Wimmer, S. Mankovsky, H. Ebert, and G. M. Stocks

Phys. Rev. B **98**, 165141 — Published 26 October 2018

DOI: 10.1103/PhysRevB.98.165141

Temperature dependent electronic transport in concentrated solid solutions of the 3*d*-transition metals Ni, Fe, Co and Cr from first principles.

G.D. Samolyuk [1*], S. Mu[1], A. F. May[1], B. C. Sales[1], S. Wimmer[2], S. Mankovsky[2], H. Ebert[2], G.M. Stocks[1]

[1] *Materials Science & Technology Division, Oak Ridge National Laboratory, Oak Ridge, TN 37831, USA*

[2] *Department of Chemistry, Ludwig-Maximilian-Universitaet, D-81377 Muenchen, Germany*

Keywords: density functional theory, alloys electronic structure, electronic transport, electrical resistivity, thermal conductivity, Nickel-based high entropy alloys, coherent potential approximation, Kubo-Greenwood formalism

AUTHOR INFORMATION

Corresponding Author

G.D. Samolyuk

* samolyukgd@ornl.gov

Abstract

An approach previously developed for the calculation of transport coefficients via the Mott relations is applied to the calculation of finite temperature transport properties of disordered alloys - electrical resistivity and the electronic part of thermal conductivity. The coherent potential approximation (CPA) is used to treat chemical disorder as well as other sources of electron scattering, i.e. temperature induced magnetic moment fluctuations and lattice vibrations via the alloy analogy model. This approach, which treats all forms of disorder on an equal first principles footing, is applied to the calculation of transport properties of a series of face-centered crystal cubic (fcc) concentrated solid solutions of the 3*d*-transition metals Ni, Fe, Co and Cr. For the nonmagnetic alloys, $Ni_{0.8}Cr_{0.2}$, and $Ni_{0.33}Co_{0.33}Cr_{0.3}$ the combined effects of chemical disorder and electron-lattice vibrations scattering result in a monotonic increase in the resistivity as a function of temperature from an already large, T=0, residual resistivity. For magnetic $Ni_{0.5}Co_{0.5}$, $Ni_{0.5}Fe_{0.5}$, $Ni_{0.33}Fe_{0.33}Co_{0.33}$, whose residual resistivity is small, additional electron scattering from temperature induced magnetic moment fluctuations results in a further rapid increase of the resistivity as a function of temperature.

The electronic part of the thermal conductivity in nonmagnetic, $Ni_{0.8}Cr_{0.2}$, and $Ni_{0.33}Co_{0.33}Cr_{0.33}$, monotonically increases with temperature. This behavior is a result of the competition between a reduction in the conductivity due to electron-lattice vibrations scattering and temperature induced increase in the number of carriers. In the magnetic alloys, electron scattering from magnetic fluctuations leads to an initial rapid decrease in thermal conductivity until this is overcome by an increasing number of carriers at temperatures slightly below the Curie temperature. Similar to the resistivity above T_C, the electronic part of the thermal conductivities are close to each other in all alloys studied.

I. INTRODUCTION

Development of a consistent, first principle transport theory is a long-standing problem in the theory of metals and alloys. In disordered alloys, depending on composition and the chemical types of the alloying elements, the electron mean free path (MFP) can be as large as hundreds of lattice parameters or as short as one (Table 1). Consequently, the interpretation of charge/heat carriers in a disordered alloys changes from well-defined long-lived quasiparticles [1], to excitations that fall outside the traditional quasiparticle description. In the latter case, transport is normally described by diffusive physics [2] and the traditional Boltzmann equation approach [1,3,4] is no longer applicable. On the other hand, the Kubo-Greenwood (KG) [5,6] approach to the calculation of the conductivity does not suffer from this problem [7] in that it deals directly with the current-current correlation function.

For disordered alloys, use of the Green's function formulation of the KG expression makes it possible to perform the necessary configurational averages of the conductivity using CPA [8,9]. This approach has an advantage of preserving the analytic properties of the conductivity within the thermodynamic limit [10,11]; albeit at the expense of the use of mean-field CPA. Implemented in conjunction with multiple scattering and density functional theory (DFT) [12], the Korringa-Kohn-Rostoker coherent-potential-approximation (KKR-CPA) [13] provides a fully *ab initio* approach to calculating transport coefficients of disordered alloys. In contrast to KKR-CPA, a recently developed approach uses DFT super-cell calculations to directly evaluate the KG expression [14,15,16]. However, for disordered alloys, configurational averaging and the thermodynamic limit must be done by hand. A similar situation pertains to another direct approach based on the results of time-dependent DFT that has been proposed and tested in the case of aluminum, by Andrade, Hamel and Carrea [17].

Initially, the KKR-CPA approach was applied to the calculation of residual resistivity where electron scattering is caused by "chemical" disorder only [11,18]. This parameter-free approach leads to a very good agreement with experimental data [19] for nonmagnetic metals. Later, the

developed approach was extended to incorporate electron scattering on lattice vibrations [20,21] and magnetic moment fluctuations [22,23] within the alloy analogy model. A similar approach was used to calculate electric, thermoelectric, and thermal transport properties of CoFe alloys based on the Kubo linear response formalism [24].

In the current work, this approach was applied to the calculation of electrical and thermal conductivity in fcc concentrated solid solutions of the 3*d*-transition metals Ni, Fe, Co and Cr . This group of alloys, including the extreme case of high entropy alloys (HEA) [25,26], demonstrates unusual transport properties [27,28,29,30]. Thus, the low temperature (T = 4 K) resistivity in these alloys varies, for example, between 1.3 $\mu\Omega \cdot cm$ in $Ni_{0.5}Co_{0.5}$ and 124.8 $\mu\Omega \cdot cm$ in NiCoFeCrPd [29]. The resistivity of NiCoFeCrPd is within the Mott-Ioffe-Regel (MIR) limit [31]. The MFP in such conductors is comparable with the interatomic distances, and transport is normally described by diffusive physics. Electrical and thermal conductivities are calculated here for Ni, $Ni_{0.5}Co_{0.5}$, $Ni_{0.5}Fe_{0.5}$, $Ni_{0.33}Co_{0.33}Fe_{0.33}$, $Ni_{0.8}Cr_{0.2}$, $Ni_{0.33}Co_{0.33}Cr_{0.33}$. The first three alloys in this group are typical representatives of low resistivity alloys $\rho < 10\ \mu\Omega \cdot cm$ and the last two alloys typify high resistivity ones, $\rho > 75\ \mu\Omega \cdot cm$ [27,28,29]. According to our estimations presented in Tab. 1, the MFP value in these alloys varies from 1689 to 4 Å and the last value is comparable to the lattice parameter (~ 3.6 Å). A unique set of properties such as significant variation of the MFP with the alloy concentration, typical metallic number of current carriers at the Fermi energy (see Table 1), almost perfect fcc lattice atomic positions, together with the fact that background properties of these alloys can be described within regular DFT [27] makes concentrated solid solutions of 3*d*-transition metals a perfect playground for the investigation of the electronic transport in general.

In Section II the approaches used to calculate electrical and thermal conductivities of alloys are presented together with experimental details of high-temperature resistivity measurements in $Ni_{0.33}Co_{0.33}Fe_{0.33}$ and $Ni_{0.35}Co_{0.35}Cr_{0.30}$. The calculated electronic structure and magnetic properties, including the temperature dependence of the magnetization and the Curie

temperatures, are presented in Section III a. In Section III b we discuss the results for electrical and thermal conductivities and we finally conclude in Section IV.

II. THEORETICAL APPROACHES, DETAILS OF CALCULATIONS AND EXPERIMENTAL PROCEDURES.

The linear response of a system to an electric field, $\vec{E}$ and (or) a temperature gradient, ∇T is characterized by electric current, $\vec{j}$, and energy flux, $\overrightarrow{J_q}$, densities and is described by the linear response equations [7]

$$\begin{aligned} e\vec{j} &= e\mathcal{L}_{11}\vec{E} - \mathcal{L}_{12}\frac{\nabla T}{T} \\ e\vec{J_q} &= e\mathcal{L}_{21}\vec{E} - \mathcal{L}_{22}\frac{\nabla T}{T}, \end{aligned} \quad \#(1)$$

where e is the electron charge. In the following formalism proposed by Chester and Thellung [32,33] based on the Mott relations [34] the transport coefficients, $\mathcal{L}_{ij}$, can be expressed as follows:

$$\mathcal{L}_{ij}^{\alpha\alpha} = (-1)^{i+j}\int d\varepsilon\sigma_{\alpha\alpha}(\varepsilon)(\varepsilon-\mu)^{i+j-2}\left[-\frac{\partial f(\varepsilon)}{\partial\varepsilon}\right], \#(2)$$

where μ is the chemical potential and $-\partial f\ (\varepsilon)/\partial\varepsilon$ is the derivative of the Fermi distribution function, and α is the Cartesian index. The above relationships may be applied to each spin channel separately. This approximation is valid in the limit of weak spin-orbit coupling as is the case for the fcc 3d-transition metal alloys that are the subject of this work. $\sigma_{\alpha\alpha}(\varepsilon)$ is calculated using the Kubo-Greenwood [5,6] expression for the static conductivity

$$\sigma_{\alpha\alpha}(\varepsilon) = \frac{\pi\hbar}{V}\langle\sum_{a,b}|\langle a|\hat{j}_\alpha|b\rangle|^2\delta(\varepsilon_a-\varepsilon)\delta(\varepsilon_b-\varepsilon)\rangle, \#(3)$$

where $\hat{j}_\alpha$ is the current operator. The quantum states $|a\rangle$ in Eq. (4) represent the exact eigenfunctions of a particular configuration of the random potential, and the large angle brackets indicate an average over configurations.

The expression for static conductivity should be reformulated using a definition of the single particle Green's function [10,11], G, as

$$\sigma_{\alpha\alpha}(\varepsilon) = -\frac{\hbar}{V\pi}\mathrm{Tr}\langle \hat{j}_\alpha \mathrm{Im}G(\varepsilon + i0)\hat{j}_\alpha \mathrm{Im}G(\varepsilon + i0)\rangle. \#(4)$$

This expression allows one to calculate transport coefficients in disordered alloys by applying the coherent potential approximation (CPA) [8,9] and multiple scattering theory formalism [13]. Details of the static conductivity calculation procedure can be found in Butler and Butler, Stocks publications [11,18].

This approach allows one to calculate the temperature dependence of both the electrical conductivity

$$\sigma_{\alpha\alpha}(T) = \mathcal{L}_{11}^{\alpha\alpha} = \int d\varepsilon \sigma_{\alpha\alpha}(\varepsilon)\left(-\frac{\partial f(\varepsilon, T)}{\partial \varepsilon}\right), \#(5)$$

and the electronic part of the thermal conductivity.

$$e^2 T\kappa_{\alpha\alpha}(T) = \mathcal{L}_{22}^{\alpha\alpha} - \frac{\mathcal{L}_{21}^{\alpha\alpha}\mathcal{L}_{21}^{\alpha\alpha}}{\mathcal{L}_{11}^{\alpha\alpha}}. \#(6)$$

Following Sommerfeld, expression (6) can be expanded to the second order in $k_B T/\mu$,

$$\kappa(T) \cong \frac{1}{3}\left(\frac{\pi}{e}\right)^2 k_B^2 T\left\{\sigma(\mu) - \frac{[\pi k_B T\sigma'(\mu)]^2/6}{\sigma(\mu) + (\pi k_B T)^2\sigma''(\mu)/6}\right\}, \#(7)$$

where $\sigma'(\mu)$ and $\sigma''(\mu)$ are the first and second energy derivatives of the static electrical conductivity. The zero order $k_B T/\mu$ contribution in Eq. (7) corresponds to the Wiedemann-Franz law (WF).

Since the chemical potential, μ, in transition metals is comparable to the width of the *d*-band ($\sim$5 eV in 3*d* metals) and we focus on intermediate temperatures ($\theta_D \leq T \leq 3\theta_D$, where θ_D is the Debye temperature, which is $\sim$400 K for the alloys discussed in the text), the condition $k_B T/\mu \ll 1$ is satisfied, and Eq. (7) is applicable if the two first derivatives of $\sigma(\mu)$ are defined.

The deviation from the WF law at low temperatures caused by non-elastic scattering or the presence of additional gapless neutral collective degrees of freedom [35,36] is not a subject of the current investigation. However, the approach presented allows one to take into account details of the electronic structure such as a complicated Fermi surface, electronic bands with nontrivial momentum dependence and broadening caused by different types of disorder including that induced by temperature.

The main contributions to the resistivity in magnetic alloys correspond to electron scattering caused by chemical disorder, magnetic moment fluctuations and lattice vibrations. By using the alloy analogy model all three scattering processes are included in the CPA resistivity calculation on an equal footing [20,21,22,23]. The details of the approach used are given in a publication by Ebert *et al.* [37]. The electronic structure of the alloys was calculated using the fully relativistic SPR-KKR-CPA method [38,39] with the angular momentum cutoff $l_{max} = 3$. The resistivity was calculated with $l_{max} = 4$. The exchange-correlation energy was calculated using both generalized gradient approximation (GGA) with the parametrization by Perdew, Burke, and Ernzerhof (PBE) [40], and local spin density approximation (LSDA) with the parametrization by Vosko, Wilk, Nusair [41]. (Later in the text the results are obtained using the PBE exchange-correlation if not specified otherwise.) Mean-square atomic displacements at different temperatures were obtained using Debye's theory with a composition-averaged Debye temperature. Neutron scattering measurements showed that the phonon dispersion in all discussed alloys is similar to that of nickel [42]. The convergence of the residual resistivity with respect to the Brillouin zone (BZ) mesh is extremely sensitive to alloy composition and components. The details of the convergence testing for the case of $Ni_{0.5}Fe_{0.5}$ and $Ni_{0.5}Co_{0.5}$ alloys can be found in the supplementary materials [43 Suppl]. According to our results, the BZ integration can be safely executed over $\sim 1.4 \times 10^5$ *k*-points in low resistivity alloys and $\sim 5 \times 10^3$ k-points in high resistivity alloys in the full BZ.

Magnetic ordering in the alloys was described by the classical Heisenberg model

$$\widehat{H} = -\sum_{i,j;i\neq j} J_{ij}\vec{e}_i\vec{e}_j, \#(8)$$

where $\vec{e}_i$ corresponds to the direction the magnetic moment on atom i and J_{ij} is the exchange coupling parameter for the atom pair (i,j). Within this model, magnetic moments are treated as rigid and the J_{ij} are calculated using a linear response approach [44] in ferromagnetic state. The averaged magnetic moments of alloy components as a function of temperature are calculated using the cluster field method (CFM) [45]. The CFM approach is equivalent [46] to the cluster variation method (CVM) [47,48] if the largest size of the clusters corresponds to pairs of atoms. It was shown [49] that the Curie temperature obtained within this approximation overestimates more accurate technique results (spin dynamics) by $\sim 10\%$.

The averaged electronic Fermi velocities $\langle v_x^2 \rangle = \langle \sum_{\vec{k},\nu} v_x^2(\vec{k},\nu)\delta(\varepsilon_{\vec{k},\nu} - E_F)\rangle$ were calculated using tight-binding linear muffin-tin orbitals (TBLMTO) [50] and the CPA formalism [51,52]. The calculated velocities were used to estimate values of the MFP through the experimental resistivity, ρ, using the expression

$$l = \frac{3}{[\rho e^2 \langle v^2 \rangle^{1/2} N(E_F)]} \#(9)$$

with electron charge, e, calculated electron velocity, $\langle v^2 \rangle^{1/2} = \sqrt{3}\langle v_x^2 \rangle^{1/2}$, and electronic density of states at the Fermi energy, $N(E_F)$. The corresponding values for this quantities are presented in Tab. 1. The underlying structure symmetry relation for the electron velocity was used in Eq. (9). In magnetic $Ni_{0.5}Co_{0.5}$, $Ni_{0.5}Fe_{0.5}$ and $Ni_{0.33}Co_{0.33}Fe_{0.33}$ alloys, the velocities and density of states of the majority spin electrons were taken into account in the MFP calculations, since electrons in the minority spin channel don't significantly contribute to the conductivity because of the large scattering in this channel.

The lattice thermal resistivity caused by phonon-phonon scattering in Ni metal, $Ni_{0.5}Co_{0.5}$, and $Ni_{0.5}Fe_{0.5}$ alloys was obtained from first-principles electronic structure calculations combined with the conventional Boltzmann transport equation and the relaxation time approximation. The thermal conductivity tensor is

$$\kappa_{\alpha\beta} = \frac{1}{V}\sum_{\lambda}\left(\partial n_{\lambda}^0/\partial T\right)\hbar\omega_{\lambda} v_{\lambda\alpha}\, v_{\lambda\beta}\tau_{\lambda\alpha}, \#(10)$$

where V is the crystal volume, α and β are Cartesian coordinates, n_λ^0 is the Bose factor, ω_λ is the phonon frequency for mode λ, $v_{\lambda\alpha}$ is the group velocity of phonon mode λ, and $\tau_{\lambda\alpha}$ is the phonon lifetime (inverse of the scattering rate) obtained from *ab initio* calculations of the phonon-phonon scattering rate (see more details in Ref. [53,54]). The lattice thermal conductivities – due to phonon-phonon scattering – are then calculated using the ShengBTE package [55]. To account for the disordered environment in alloys, the virtual crystal approximation was employed. This approximation does not include phonon scattering resulting from mass or force disorder (see discussion). The Harmonic force constants were estimated using DFPT as implemented in QUANTUM ESPRESSO (QE) [56]. In addition, third order force constants were evaluated based on a 64-atom rhombohedral unit cell using the *ab initio* finite difference method in QE. PBE parametrization is used for exchange and correlation in all calculations. The ultra-soft pseudopotential [57] was employed with the plane wave cut-off equal to 32 Ry. The Brillouin Zone (BZ) integration was performed using γ-center 16×16×16 (2×2×2) k-point meshes for primitive cell density functional perturbation [58,59] theory calculations and supercell calculations, respectively.

The electrical resistivity of $Ni_{0.33}Co_{0.33}Fe_{0.33}$ and $Ni_{0.35}Co_{0.35}Cr_{0.3}$ was measured to approximately 1060 K using a four-point configuration [60] with platinum wires spot welded to the samples. Currents of 0.5 mA and 1.0 mA were employed with alternating bias direction for the measurements of $Ni_{0.35}Co_{0.35}Cr_{0.3}$ and $Ni_{0.33}Co_{0.33}Fe_{0.33}$, respectively. The temperature was monitored with two type-E thermocouples and an average value is reported, the measurements were performed in an argon atmosphere. The data were collected using a Keithley 220 current source and a Keithley 2182 nanovoltmeter with facilitation by a python code. In these resistivity measurements the samples were a single crystal. The composition of the experimental $Ni_{0.35}Co_{0.35}Cr_{0.3}$ sample is slightly different from the one used in theoretical calculations, $Ni_{0.33}Co_{0.33}Cr_{0.33}$, but, according to calculations, this small difference in concentration modifies the residual resistivity by no more than 2%.

III. RESULTS AND DISCUSSION

a. Electronic structure and magnetic properties

The investigated concentrated solid solutions are naturally separated into two groups – alloys in one group contain Cr (typical representatives are $Ni_{0.8}Cr_{0.2}$ and $Ni_{0.33}Co_{0.33}Cr_{0.33}$) and alloys from the second group don't. It should be mentioned that despite the applicability of DFT, self-consistent calculations of $Ni_{0.33}Co_{0.33}Cr_{0.33}$ converged to a magnetic ground state in both supercell and CPA approaches experimentally this alloy is nonmagnetic. In addition, $NiCoCr_x$ exhibits quantum critical behavior near x=0.8 [61].

To be consistent with experimental results, the $Ni_{0.33}Co_{0.33}Cr_{0.33}$ alloy was treated in our calculations as nonmagnetic. The details of the electronic structure of the group of alloys were discussed in our previous publications [27,62,63]. For the convenience of the readers, the discussion is reproduced for $Ni_{0.5}Co_{0.5}$ and $Ni_{0.8}Cr_{0.2}$. The spin-resolved electronic density of states (DOS) are shown in Fig. 1(a) and Fig. 1 (b) for Co and Cr containing alloys respectively (DOS for the rest of alloys can be found in supplementary materials [43]). In the figure, the Fermi energy is taken as zero. For each alloy panel, the left (right) panels correspond to the DOS of majority (minority)-spin states, respectively. Within each panel, the solid red (dashed blue) lines correspond to the Ni (second-species) local DOS respectively. Similarly, the horizontal solid red (dashed blue) lines denote the centers of gravity of the Ni (second-species) spin-resolved *d*-band center of the corresponding species. It equals the resonance energy E_d of the *d*-wave (angular momentum channel $l = 2$) scattering phase shift δ_d i.e. the energy satisfying the conditions $\delta_d(E_d) = \pi/2$ (see discussion in our previous publications [62,63]). A Cr atom contains five *d*-electrons and has a half-filled *d*-bands whereas Fe, Co, and Ni belong to the group of transition metals with an almost filled *d*-band. This results in different magnetic exchange coupling – 3*d*-transition metals with almost filled *d*-bands have a tendency to ferromagnetic ordering, while metals with half-filled bands tend to exhibit antiferromagnetic ordering [64,65]. Additionally, the electronic structure of metals from these two groups behave differently upon alloying. The occupation of *d*-bands and the resulting position of the Fermi level can be approximately obtained by minimization of the band structure energy, E_b, together with additional constraints to preserve atomic charge neutrality. In alloys with a close number

of *d*-electrons (Fe, Co, Ni) E_b minimization results in the alignment of majority spin *d*-states in $Ni_{0.5}Co_{0.5}$ with almost negligible splitting, Δ, between Ni and Co *d*-bands centers ($\Delta/W \ll 1$, where W is the *d*-bandwidth). This corresponds to weak scattering in the majority spin channel and a low resistivity in this channel. This weak scattering creates a "shortcut" for the electrical current resulting in a small total residual resistivity typical for high conductivity alloys. The scattering in the minority spin channel can be estimated from the relation between exchange splitting and the size of the magnetic moment of each element [62]. The large difference in the number of *d*-electrons in Cr and Ni doesn't allow alignment of the *d*-bands of each component while preserving atomic charge neutrality. Together with an absence of spin polarization, this results in a large *d*-band splitting $\Delta = 0.73$ eV in both spin channels with significant electron scattering and, as a result, a large residual resistivity. These conclusions agree with experimental observations [27,29] that all compounds containing Cr belong to the low conductivity group. This analysis can easily be extended to alloys containing more than two components [63].

Important information about the character of electron dynamics in an alloy can be obtained from the values of the MFP. In the current publication the MFP was estimated from the resistivity using Eq. (9). Since the main channel for electron propagation in magnetic alloys corresponds to majority spin states, the corresponding Fermi velocity, $\langle v_x^2(E_F)\rangle^{1/2}$ and density of states, $N(E_F)$, are used in Eq. (9). In magnetic alloys, the electronic states at the Fermi level in the majority spin channel correspond to *sp*-electrons (see Fig. 1(a)) with a high velocity of 0.46×10^6 m/s (Table 1) that is only weakly dependent on the chemical composition. Whereas in nonmagnetic Cr containing alloys, the electronic states correspond to *d*-electrons with low energy dispersion (see Fig. 1(b)) and the corresponding velocities are almost a factor of two lower (0.24×10^6 m/s) than in magnetic alloys. The MFP calculated for $Ni_{0.5}Co_{0.5}$ equals 1690 Å and is comparable to the values for pure transition metals, which is not surprising since the electronic structure of a $Ni_{0.5}Co_{0.5}$ alloy can be described within the virtual crystal approximation with high accuracy [27,62]. The MFP in $Ni_{0.5}Fe_{0.5}$ and $Ni_{0.33}Co_{0.33}Fe_{0.33}$ are significantly smaller, 174 and 478 Å, respectively. However, in all three of these alloys, the calculated MFP is significantly larger than the lattice parameter of ~ 3.6 Å, and consequently

electronic transport in the alloys containing all components with almost filled *d*-electrons states can be interpreted as a propagation of well-defined quasiparticles obeying the Boltzmann equation [66,67,68]. In contrast to this group of alloys, the presence of Cr dramatically increases electron scattering and reduces the MFP to values equal to 4.1 and 4.0 Å in $Ni_{0.8}Cr_{0.2}$ and $Ni_{0.33}Co_{0.33}Cr_{0.33}$, respectively. These values are comparable with the lattice parameter and hence the applicability of the Boltzmann equation to electron transport in these alloys is questionable. As we mentioned in the Introduction, the KG formalism allows one to calculate both the electronic and thermal conductivity without such limitations. For convenience of the readers, the calculated results for residual resistivity, already published in work by S. Mu, G. Samolyuk et al [63], are reproduced in Table 1. As can be seen for the case of iron containing alloys, the LSDA result is ~30% large than the GGA one. For the rest of alloys LSDA and GGA results are close to each other. Detailed discussion of residual resistivity results and comparison with experiment can be find in reference [63].

In the magnetic alloys the contribution of electron scattering by temperature dependent magnetic moment fluctuations to the electrical and thermal conductivity was calculated using the Heisenberg model, Eq.(8) and the averaged value of the magnetic moment as a function of temperature. The calculated zero temperature values of the magnetic moments are weakly dependent on alloy composition and are approximately $0.6\mu_B$, $1.6\mu_B$ and $2.5\mu_B$ for Ni, Co and Fe, respectively (Tab. 1). The range of the calculated exchange couplings, J_{ij}, in alloys doesn't exceed 1.8 lattice parameters (see supplementary materials [43]) and 2.0 lattice parameters in pure Ni. In the current calculations, all atomic magnetic moments were treated as rigid vectors and the well-known longitudinal fluctuations of Ni [69,70] were not taken into account. This results in a significantly underestimated Curie temperature, T_C, for pure Ni [44,64] — 342 K, calculated using the PBE parametrization of the exchange-correlation energy versus the experimental value of 628 K. Below, for the calculation of conductivity, the temperature dependence of the magnetization for pure Ni was rescaled by the experimental Curie temperature. In the alloys the dominant magnetic interaction corresponds to Fe or Co atoms. For these elements, the rigid spin approximation is a very reasonable approach [69] and the calculated Curie temperatures are in much better agreement with experiment. The Curie

temperatures were overestimated by 6% in $Ni_{0.5}Co_{0.5}$ and by 20% in $Ni_{0.5}Fe_{0.5}$ and $Ni_{0.33}Co_{0.33}Fe_{0.33}$ alloys. Curie temperatures obtained within local spin density approximation (LSDA) are 10-20% lower compared to GGA PBE ones. The calculated magnetic transition in all alloys is of second order.

b. Results for transport properties

The electronic part of the alloy thermal conductivity is calculated using Onsager relations for the transport coefficients, $\mathcal{L}_{ij}^{\alpha\alpha}$, Eq. (6), where $\mathcal{L}_{ij}^{\alpha\alpha}$ are obtained through integration over energy of the static conductivity and the derivative of the Fermi distribution function, Eq. (2). At low temperatures the approximate Eq. (7) is used. A necessary condition for the application of expression (7) for the thermal conductivity is "well behaved" on an energy scale of half-width of the derivative of the Fermi function at temperature T. In Fig. 2 the energy dependence of zero temperature $\sigma(E)$ is presented for $Ni_{0.5}Co_{0.5}$, $Ni_{0.5}Fe_{0.5}$ and $Ni_{0.8}Cr_{0.2}$. Because of large scattering in both spin channels, $\sigma(E)$ in $Ni_{0.8}Cr_{0.2}$ is a smooth function. While for $Ni_{0.5}Co_{0.5}$ and $Ni_{0.5}Fe_{0.5}$, $\sigma(E)$ changes non-monotonically near the Fermi energy. Such a behavior is caused by the Ni, Co, Fe majority spin states alignment as discussed above in the text. As a result, electron scattering in this spin channel is weak and electron excitations are well-defined long-living quasiparticles described by "zero" thickness bands. This results in the presence of fine structure in the electronic density of states around the Fermi energy, which is dominated by *d*-states. In these alloys the applicability of Eq. (7) is questionable. However, $\sigma(E)$ in Eq. (6-7) should be calculated at some particular temperature and should include the effects of electron scattering on the temperature-induced magnetic moment fluctuations as well as lattice vibrations. After incorporation of scattering on just magnetic moment fluctuations, the character of the conductivity energy dependence changes dramatically, see Fig. 3. In $Ni_{0.5}Co_{0.5}$ this dependence changes from a set of sharp peaks to a slowly monotonically growing function. Thus, even in the worst case of $Ni_{0.5}Co_{0.5}$ Eq. (7) is applicable and is used in our calculations.

(i) Results for pure Ni

The results for the resistivity of pure Ni are consistent with previously published ones [37]. Below the Curie temperature the calculated resistivity, shown by a red solid line with filled circles in Fig. 4 (a), systematically overestimates the experimental values [28] by $\sim 10\ \mu\Omega \cdot \mathrm{cm}$. The reason for this difference is a discrepancy between the experimental temperature dependence of the magnetization and the magnetization calculated from the classical Heisenberg model. The calculated magnetization decreases with temperature faster than the experimental magnetization [71] (insert in Fig. 4 (a)), and, as a result, electron scattering on magnetic moment fluctuations is overestimated. To prove this statement, the experimental magnetization temperature dependence [71] is also used to calculate the resistivity (shown by green line with filled down triangles). The deviation from the experimental results in this case is below 15% for temperatures up to 400 K. As the temperature approaches T_C the deviation from experiment doubles in both types of calculations. This deviation is a result of the rigid magnetic moment used in our calculation. The electron scattering by fluctuations of fully disordered magnetic moments of $0.6\mu_B$ is significantly larger than the moment fluctuations of 0.3-0.4 μ_B experimentally observed near the Curie temperature. (see [72] and reference therein).

Following the publication by Ebert *et al.* [37], above the Curie temperature the resistivity is calculated in the nonmagnetic state. The resistivity in this case is defined by electron scattering on lattice vibrations only. The calculated resistivity is in perfect agreement with experiment above T_C.

The electronic part of the thermal conductivity calculated from the zero order $(k_B T/\mu)$ term in Eq. (7) (corresponding to the WF law) and the theoretical magnetization, is shown by a red line with filled circles in Fig. 4(b). The full calculated electronic κ, including second order $(k_B T/\mu)$ corrections, is shown by empty diamonds. The derivatives of $\sigma(E)$ used in Eq. (7) were calculated numerically. As can be seen, there is no visual difference between these two sets of data at most temperatures, except a few percent deviations from WF at temperatures between 550 K and T_C. The lattice contribution to the thermal conductivity is shown by a blue line with open circles. Its temperature dependence could be approximately described by a power law,

$1/T^{\alpha}$, where $\alpha = 0.97$, is close to 1. This behavior of lattice thermal conductivity is very typical for ordered materials with the main source of phonon scattering coming from the three-phonon interaction. The total thermal conductivity is shown by a green line with filled down triangles. The calculated thermal conductivity above T_C is in excellent agreement with experiment. This isn't surprising since the calculated resistivity reproduces the experiment with high accuracy. Below the Curie temperature, the calculated thermal conductivity is underestimated by ~ 20 W/(m K). This is the result of the overestimated electrical resistivity. The total thermal conductivity calculated using the electronic part of the conductivity obtained from experimental magnetization data (green triangles in Fig. 4 (a)) is shown by a grey line with filled squares. Similar to the resistivity case, incorporation of the experimental temperature dependence of the magnetization significantly improves agreement with experiment for all temperature regions except the interval between 550 K and T_C, where the longitudinal nickel magnetic moment fluctuations play an important role.

(ii) Results for the ferromagnetic $Ni_{0.5}Co_{0.5}$, $Ni_{0.5}Fe_{0.5}$ and $Ni_{0.33}Co_{0.33}Fe_{0.33}$

Results of resistivity calculations for $Ni_{0.5}Co_{0.5}$ alloys are presented in Fig. 5 (a). The magnetization as a function of temperature for both alloy components was calculated by solving the classical Heisenberg model within the CFM approach. Similar to the case of nickel, this approach overestimates the rate of magnetization reduction with the temperature increase as compared to experiment. This results in an overestimation of the calculated resistivity compared to available experimental data [28]. Cobalt is the main magnetic component in this alloy. The longitudinal fluctuations of the Co magnetic moment are much smaller compared to nickel [68] and hence the rigid moment approximation used in the calculations is justified. Thus in the temperature interval between 200 degrees below and above T_C much better agreement between the calculated resistivity and experiment is expected. This expectation is supported by very good agreement between the calculated and experimental thermal conductivity [29] in this interval of temperatures as shown in Fig. 5 (b) by a green line with down triangles for the calculated result and up cyan triangles for the experiment. Results for the calculated lattice contribution were obtained within the virtual crystal approximation, which has limited

applicability. It includes three-phonon scattering only and neglects phonon scattering on lattice disorder introduced by a random distribution of different types of atoms in the alloy. As was shown by Alam and Mookerjee [73], the temperature dependence of the lattice thermal conductivity, defined by phonon scattering on lattice disorder, is very different from the three-phonon scattering result. The alloy lattice thermal conductivity starts from zero at low temperatures and monotonically increases with the temperature until saturation is reached. However, above $2\theta_D$ three-phonon scattering dominates. At these temperatures, the VCA can be used to estimate the lattice thermal conductivity, and as can be seen from Fig. 5 (b), at these temperatures there is reasonable agreement between theory (green line with down triangles) and experiment (cyan color up triangles).

Results for the calculated resistivity in $Ni_{0.5}Fe_{0.5}$ and $Ni_{0.33}Co_{0.33}Fe_{0.33}$ are very similar to the results obtained for $Ni_{0.5}Co_{0.5}$. It has a nonzero value at zero temperature, corresponding to the residual resistivity, caused by electron scattering on the chemical disorder. Because of majority spin states alignment, as discussed in the previous section, the scattering in this channel is small and the residual resistivity is below $10\ \mu\Omega \cdot cm$ – a values typical for low resistivity alloys. As temperature increases, the resistivity increases with approximately the same rate and reaches $\sim 100\ \mu\Omega \cdot cm$ at the Curie temperature, which is between 900 and 1150 K for all three alloys. The rapid increase of resistivity for temperatures below the Curie temperature is determined by increased scattering by magnetics fluctuations. Above the Curie temperature, the magnetic moment disorder reaches saturation when the averaged projection of the magnetic moment to the z-direction equals zero, and the strength of electron scattering on magnetic moment fluctuations also saturates. The temperature dependence of the resistivity above T_C is determined by the electron scattering on lattice vibrations, which grow linearly with temperature. As a result, above T_C the resistivity slowly rises with temperature. It is worthwhile to mention that the highest values of resistivity are close to the MIR limit. In the limit the electron mean free path is comparable to an interatomic spacing, the resistivity reaches saturation. However, this resistivity saturation never has been reached in both calculations and high-temperature experiments for $Ni_{0.33}Co_{0.33}Fe_{0.33}$, as shown by cyan triangles in Fig. 7 (a). The low-temperature experimental data (below 300 K) are taken from Ref. [28],

while data above 300 K has been obtained in the current work. Agreement between experiment and theory is reasonably good. Thus around the Curie temperature the calculations reproduce the experimental resistivity with a few percent accuracy. At temperatures below 700 K deviation from experiment is more significant. The calculated resistivity increases with temperature much faster at low temperatures compared to experiment. Similar to nickel, this inconsistency is a result of the overestimated rate of magnetic moment projection reduction with the temperature increase as calculated by solving the classical Heisenberg model. Surprisingly, the calculated resistivity in $Ni_{0.5}Fe_{0.5}$ at temperatures between 200 K and 400 K is in much better agreement with experiment, Fig. 6a, than in $Ni_{0.5}Co_{0.5}$ and $Ni_{0.33}Co_{0.33}Fe_{0.33}$. This difference is caused by the much larger discrepancy between calculated, 2.45 μΩ·cm, and experimental, 10.37 μΩ·cm, residual resistivities (see Table 1). As a result, even if calculated resistivity rises faster than the experimental one, due to smaller zero temperature value, the calculated resistivity began to be very close to the experimental at approximately 200 K and above. The difference between calculated and experimental residual resistivities is discussed in detail in work by S. Mu et al [63].

The thermal conductivity temperature dependence is also very similar in all three alloys. It starts from values $50 - 65$ W/(m K) at approximately 200 K and monotonically decreases until reaching values $30 - 45$ W/(m K) at temperature T´ approximately 200 K below T_C. This decrease is a result of the increase in electron scattering by magnetic moment fluctuations and lattice vibrations with increasing temperature, the scattering strength grows faster than the number of heat carriers, which is proportional to temperature (T coefficient in Eq. (8)). Above T´ the thermal conductivity behavior changes and begins to increase with increasing temperature. This change in behavior is caused by the increasing number of heat carriers, which overcomes the conductivity decrease caused by electron scattering. This is primarily because scattering by magnetic moment fluctuations saturates. Similar to $Ni_{0.5}Co_{0.5}$ the correction to the WF law, shown by white diamonds in Fig. 6 (b) and 7 (b), can be neglected. However, in contrast to the $Ni_{0.5}Co_{0.5}$ alloy, the calculated thermal conductivity in $Ni_{0.5}Fe_{0.5}$ is overestimated by approximately 20% at temperatures above $2\theta_D$. For $Ni_{0.33}Co_{0.33}Fe_{0.33}$ the calculated thermal

conductivity behaves like the averaged value of the $Ni_{0.5}Co_{0.5}$ and $Ni_{0.5}Fe_{0.5}$ conductivities and is in surprisingly good agreement with experiment.

Further, the experimental resistivity was used to calculate the electronic part of the thermal conductivity by applying the WF law and this was used as an input for the total thermal conductivity. The result is shown by grey squares in Fig. 7 (b). As can be seen, the agreement with experiment is not as good as for the conductivity obtained from the calculated magnetization. The total κ deviates from the experimental data below 700 K and this deviation increases with temperature reduction. Since, as was demonstrated above, the deviations from the WF law are negligible, the source of this disagreement should be attributed to an overestimated lattice thermal conductivity calculated within the VCA.

(iii) Results for the nonmagnetic $Ni_{0.8}Cr_{0.2}$ and $Ni_{0.33}Co_{0.33}Cr_{0.33}$

The results for electrical resistivity in two representatives of high-resistivity alloys, $Ni_{0.8}Cr_{0.2}$ and $Ni_{0.33}Co_{0.33}Cr_{0.33}$, are presented in Fig. 8 (a) and 9 (a). Both alloys are nonmagnetic, consequently, the magnitude and temperature dependence of the conductivity is determined by electron scattering on chemical disorder and lattice vibrations only. As a result the temperature dependence of the electrical resistivity is much simpler. It starts from $\sim 80\ \mu\Omega \cdot cm$ (residual resistivity) and monotonically increases with the temperature (red line with filled dots in Fig. 8 (a) and 9 (a)). The resistivity increase is slower in $Ni_{0.8}Cr_{0.2}$, by 7.8 $\mu\Omega \cdot cm$ for the temperature interval between 100 and 1200 K, than for $Ni_{0.33}Co_{0.33}Cr_{0.33}$, which increases by 16.6 $\mu\Omega \cdot cm$ over the same temperature interval. The slope of resistivity temperature dependence in $Ni_{0.33}Co_{0.33}Cr_{0.33}$ is slightly lower than the experimental slope as shown by triangles in Fig. 9 (a). Also, the experimental slope slightly changes at 800 K. This transition is traditionally attributed to a K-state transition and it has been previously observed in experimental specific heat capacity measurements [29]. It should be mentioned that even while the resistivity starts at much higher values for low temperatures in Cr containing alloys, the so-called high resistivity alloys, at about 1000 K the resistivity values are similar in all of the discussed solid solutions. In low-resistivity alloys the absence of large electrons scattering on

chemical disorder is compensated by electron scattering on magnetic moment fluctuations increasing with temperature.

The results for the thermal conductivity in these two alloys are presented in Fig. 8 (b) and 9 (b) by the filled red circles together with the correction to the WF law as shown by empty diamonds. Similar to the case of the low-resistivity alloys, there is no significant deviation from the WF law. In $Ni_{0.8}Cr_{0.2}$ the calculated electronic part of the thermal conductivity (Fig. 8 (b)) is 5 W/(m K) lower than the experimental one at temperatures below 700 K, shown by blue triangles. Above 700 K, according to our results, the lattice contribution to the total conductivity equals zero. This result looks especially surprising taking into account the fact that traditionally, it is supposed that in highly disordered systems the phonon contribution to the total thermal conductivity is larger than the electronic one [74]. The possible reason for this disagreement is in an underestimated calculated resistivity. However, the absence of experimental data does not allow us to justify this assumption.

A similar result was obtained in $Ni_{0.33}Co_{0.33}Cr_{0.33}$ (Fig. 9 (b)). The calculated electronic part of the thermal conductivity, shown by a red line with filled circles, equals the total experimental conductivity at 600 K and below, and slightly larger than the experiment above this temperature. The reason for this discrepancy is that the calculated electrical resistivity is approximately 10 $\mu\Omega \cdot cm$ lower than the experimental one (Fig. 9 (a)). The electronic part of the thermal conductivity calculated from the experimental electrical resistivity using the WF law (grey squares in Fig. 9 (b)) is in better agreement with experiment. In all intervals of the temperature it is lower than the total experimental thermal conductivity. According to the calculations, the contribution from the lattice conductivity equals 5 W/(m K) at room temperature and is reduced to approximately 2 W/(m K) at the highest temperatures. However, similar to $Ni_{0.8}Cr_{0.2}$, the lattice contribution is unexpectedly small.

IV. CONCLUSIONS

The formalism proposed by Chester and Thellung for the calculation of transport coefficients of Mott relations was applied to the calculation of alloy transport properties -

electrical resistivity and the electronic part of the thermal conductivity. The electrical conductivity is used as an input for the calculation of thermal transport properties. The electrical conductivity was calculated using the Kubo-Greenwood formalism where the coherent potential approximation was applied to obtain the alloy Green's function. This approach allows for a consistent calculation of the properties of disordered alloys using configurational averaging and the thermodynamic limit. All sources for electron scattering, i.e. chemical disorder, and temperature induced magnetic moment fluctuations and lattice vibrations are included in the CPA scheme on equal footing using the alloy analogy model. This allows one to take into account details of the electronic structure such as a complicated Fermi surface, electronic bands with nontrivial momentum dependence and broadening caused by disorder. In the current work this approach was applied to the calculation of transport properties of the series of fcc concentrated solid solutions of the 3*d*-transition metals Ni, Fe, Co and Cr . Reasonable agreement with experimental data was obtained. It was demonstrated that in all alloys in the temperature interval of $\theta_D \leq T \leq 3\theta_D$ the deviation from the Wiedemann-Franz law is insignificant. This is because of the smearing of features in the electronic structure by temperature-induced magnetic moment fluctuations and lattice vibrations.

For the nonmagnetic alloys, $Ni_{0.8}Cr_{0.2}$ and $Ni_{0.33}Co_{0.33}Cr_{0.3}$ the combined effect of chemical disorder and electron-phonon scattering results in a monotonic increase in the resistivity as a function of temperature starting from a large residual resistivity. For magnetic $Ni_{0.5}Co_{0.5}$, $Ni_{0.5}Fe_{0.5}$, $Ni_{0.33}Fe_{0.33}Co_{0.33}$ alloys, the residual resistivity is small, but additional electron scattering from temperature induced magnetic moment fluctuations results in a rapid increase of the resistivity as a function of temperature. Above the Curie temperature the electron scattering by magnetic moment fluctuations saturates and the resistivity slowly increases due to electron-phonon scattering.

The electronic part of the thermal conductivity in nonmagnetic high-resistivity alloys, $Ni_{0.8}Cr_{0.2}$ and $Ni_{0.33}Co_{0.33}Cr_{0.33}$, monotonically increases with temperature. This behavior is a result of competition between conductivity reduction caused by electron-phonon scattering and temperature induced increase of the number of heat carriers. In magnetic low-resistivity

alloys, the presence of magnetic fluctuations results in a rapid reduction of the thermal conductivity until this reduction is overcome by an increasing number of carriers at temperatures slightly below the Curie temperature. Similar to the resistivity, above T_C the electronic part of the thermal conductivities are similar in all investigated alloys.

V. ACKNOVLEDGMENTS

Work was performed at the Energy Dissipation to Defect Evolution Center, an Energy Frontier Research Center funded by the U.S. Department of Energy (Award Number 2014ORNL1026) at Oak Ridge Laboratories. BCS and AFM were supported by DOE, Office of Science, Basic Energy Sciences, Materials Sciences and Engineering Division. Authors used resources of the National Energy Research Scientific Computing Center, which is supported by the Office of Science of the US Department of Energy. The authors would like to thank A. Strange for critical reading of the manuscript. SW, SM, and HE would like to thank the DFG (Deutsche Forschungsgemeinschaft) for financial support within the priority program SPP 1538 and the collaborative research centers 689 and 1277.

LIST OF LITERATURE

1) J. M. Ziman, Electrons and Phonons, The Theory of Transport Phenomena in Solids (Oxford Univ. Press, Oxford, 1960)
2) S. A. Hartnoll, Theory of universal incoherent metallic transport, Nature Phys. **11**, 54 (2015).
3) P. B. Allen, Phys. Rev. B **17**, 3725 (1978).
4) S. Y. Savrasov and D. Y. Savrasov, Phys. Rev. B *54*, 16487 (1996).
5) R. Kubo, J. Phys. Soc. Jpn. **12**, 570 (1957).
6) D. A. Greenwood, Proc. Phys. Soc. London **71**, 585 (1958).
7) [MAHAN] G.D. Mahan, *Many-Particles Physics*, Physics of Solids and Liquids (Springer, New York, 2000).
8) P. Soven, Phys. Rev. **156**, 809 (1967).
9) W.D. Taylor, Phys. Rev. **156**, 1017 (1967).
10) B. Velicky, Phys. Rev. **184**, 614 (1969).
11) W.H. Butler, Phys. Rev. B **31**, 3260 (1985).
12) W. Kohn, L. J. Sham, Phys. Rev. **140**, A1133–A1138 (1965).
13) G.M. Stocks, W.M. Temmerman, and B.L. Gyorffy, Phys.Rev. Lett. **41**, 339 (1978).
14) V. Recoules, J.-P. Crocombette, Phys. Rev. B **72**, 104202 (2005).
15) S. Mazevet, M. Torrent, V. Recoules, F. Jollet, High Energy Density Physics **6**, 84-88 (2010).
16) M. Pozzo, M. P. Desjarlais, and D. Alfè, Phys. Rev. B **84**, 054203 (2011).
17) X. Andrade, S. Hamel, and A. A. Correa, arXiv:1702.00411v1.
18) W.H. Butler, and G.M. Stocks, Phys. Rev. B **29**, 4217 (1984).
19) P. B. Allen, T. P. Beaulac, F. S. Khan, W. H. Butler, F. J. Pinski, and J. C. Swihart, Phys. Rev. B **34**, 4331 (1986).
20) H. Ebert, S. Mankovsky, D. Ködderitzsch, and P. J. Kelly, Phys. Rev. Lett. **107**, 066603 (2011).
21) D. Ködderitzsch, K. Chadova, J. Minár, and H. Ebert, New J. Phys. **15**, 053009 (2013).

22) J. Kudrnovský, V. Drchal, I. Turek, S. Khmelevskyi, J. K. Glasbrenner, and K. D. Belashchenko, Phys. Rev. B **86**, 144423 (2012).

23) S. Mankovsky, D. Ködderitzsch, G. Woltersdorf, and H. Ebert, Phys. Rev. B **87**, 014430 (2013).

24) S. Srichandan, S. Wimmer, M. Kronseder, H. Ebert, C. H. Back, and C. Strunk, arXiv:1802.01038v1

25) B. Cantor, I.T.H. Chang, P. Knight, and A. J. B. Vincent, Mater. Sci. Eng. A **375**, 213–218 (2004).

26) B. Cantor, Stable and metastable multicomponent alloys. in Annales de chimie **32**, 245–256 (2007).

27) Y. Zhang, G.M. Stocks, K. Jin, C. Lu, H. Bei, B.C. Sales, L. Wang, L.K. Beland, R.E. Stoller, G.D. Samolyuk, M. Caro, A. Caro, W.J. Weber, Nat. Commun. **6**, 8736 (2015).

28) K. Jin, B.C. Sales, G.M. Stocks, G.D. Samolyuk, M. Daene, W.J. Weber, Y. Zhang, H. Bei, Sci. Rep. **6**, 20159 (2016).

29) K. Jin, S. Mu, K. An, W.D. Porter, G.D. Samolyuk, G.M. Stocks, H. Bei, Materials and Design **117**, 185 (2017).

30) B. C. Sales, K. Jin, H. Bei, G. M. Stocks, G. D. Samolyuk, A. F. May, M. A. McGuire, Sci. Rep. **6**, 26179 (2016).

31) O. Gunnarsson, M. Calandra, J.E. Han, Colloquium: Saturation of electrical resistivity, Rev. Mod. Phys. **75**, 1085-1099 (2003).

32) G.V. Chester, and A. Thellung, Proc. Phys. Soc. **77**, 1005 (1961).

33) M.J. Kearney, and P.N. Butcher, J Phys. C: Solid State Phys. **21**, L265-L270 (1988).

34) S. N. F. Mott and H. Jones, The Theory of the Properties of Metals and Alloys, Courier Dover Publications, 1958.

35) R. Mahajan, M. Barkeshli, S. A. Hartnoll, Phys. Rev. B **88**, 125107 (2013).

36) K.-S. Kim, and C. Pépin, Phys. Rev. Lett. **102**, 156404 (2009).

37) H. Ebert, S. Mankovsky, K. Chadova, S. Polesya, J. Minár, and D. Ködderitzsch, Phys. Rev. B **91**, 165132 (2015).

38) H. Ebert, D. Ködderitzsch, and J. Minár, Rep. Prog. Phys. **74**, 096501 (2011).

39) The Munich SPR-KKR package, version 7.7, H. Ebert et al., http://olymp.cup.uni-muenchen.de/ak/ebert/SPRKKR (2017).

40) J.P. Perdew, K. Burke, and M. Ernzerhof, Phys. Rev. Lett. **77**, 3865 (1996).

41) S. H. Vosko, L. Wilk, M. Nusair, Canadian J. of Phys. **58**, 1200 (1980).

42) S. Mu, R. Olsen, B. Dutta, B. C. Larson, L. Lindsay, G. D. Samolyuk, E. D. Specht, K. Jin, H. Bei, T. Berlijn, T. Hickel, and G. M. Stocks, to be published.

43) Supplementary Material at ...

44) A. I. Liechtenstein, M. I. Katsnelson, V. P. Antropov, and V. A. Gubanov, J. Magn. Magn. Mater. **67**, 65 (1987).

45) V. G. Vaks, and N. E. Zein, Sov. Phys. JETP **40**, 537, (1975).

46) V.G. Vaks, and G.D. Samolyuk, JETP **88**, 89-100 (1999).

47) R. Kikuchi, Phys. Rev. **81**, 988 (1951).

48) J. M. Sanchez, F. Ducastelle, and D. Gratias, Physica A **128**, 334 (1984).

49) J. L. Xu, M. van Schilfgaarde, and G.D. Samolyuk, Phys. Rev. Lett. **94**, 097201 (2005).

50) O.K. Andersen, and O. Jepsen, Phys. Rev. Lett. **53**, 2571 (1984).

51) I.A. Abrikosov and H.L. Skriver, Phys. Rev. B **47**, 16532–41 (1993).

52) I. Turek, V. Drchal, J. Kudrnovský , M. Sŏb, and P. Weinberger*, Electronic Structure of Disordered Alloys, Surfaces and Interfaces* (Kluwer, Boston, 1997).

53) D. A. Broido, M. Malorny, G. Birner, N. Mingo, and D. A. Stewart, Appl. Phys. Lett. **91**, 231922 (2007).

54) D. A. Broido, L. Lindsay, and A. Ward, Phys. Rev. B **86**, 115203 (2012).

55) W. Li, J. Carrete, N, A. Katcho, and N. Mingo, Comp. Phys. Commun. **185**, 1747 (2014).

56) P. Giannozzi, S. Baroni, N. Bonini, M. Calandra, R. Car, C. Cavazzoni, D. Ceresoli, G. L. Chiarotti, M. Cococcioni, I. Dabo, A. D. Corso, S. de Gironcoli, S. Fabris, G. Fratesi, R. Gebauer, U. Gerstmann, C. Gougoussis, A. Kokalj, M. Lazzeri, L. Martin-Samos, N. Marzari, F. Mauri, R. Mazzarello, S. Paolini, A. Pasquarello, L. Paulatto, C. Sbraccia, S. Scandolo, G. Sclauzero, A. P. Seitsonen, A. Smogunov, P. Umari, R. M. Wentzcovitch, J. of Phys.: Cond. Matter **21**, 395502 (2009).

57) D. Vanderbilt, Phys. Rev. B **41**, 7892 (1990).

58) N.E. Zein, Sov. Phys. Solid State **26**, 1825 (1984).

59) S. Baroni, P. Giannozzi, and A. Testa, Phys. Rev. Lett. **58**, 1861 (1987).

60) E.H. Putley, The Hall Effect and Related Phenomena (Butterworths, London, 1960).

61) B. C. Sales, K. Jin, H. Bei, J. Nichols, M. F. Chisholm, A. F. May, N. P. Butch, A. D. Christianson, and M. A. McGuire, npj Quantum Materials **2**, 33 (2017).

62) G. D. Samolyuk, L. K. Béland, G. M. Stocks and R. E. Stoller, J. Phys.: Condens. Matter **28**, 175501 (2016).

63) S. Mu, G. D. Samolyuk, S. Wimmer, M. C. Troparevsky, S. Khan, S. Mankovsky, H. Ebert, G. M. Stocks, arXiv:1806.03785.

64) M. van Schilfgaarde, V. P. Antropov J. of Appl. Phys. **85**, 4827 (1999); doi.org/10.1063/1.370495

65) G. D. Samolyuk, B. P. T. Fokwa, R. Dronskowski, and G. J. Miller, Phys. Rev. B **76**, 094404 (2007).

66) G. Baym and L. P. Kadanoff, Phys. Rev. **124**, 287 (1961).

67) R. E. Prange, L. E. Kadanoff, Phys. Rev. **134**, A566 (1964).

68) T. Holstein, Annals of Phys. **29**, 410-535 (1964).

69) A. V. Ruban, S. Khmelevskyi, P. Mohn, and B. Johansson, Phys. Rev. B **75**, 054402 (2007).

70) V. Drchal, J. Kudrnovský, and I. Turek, EPJ Web of Conferences **40**, 11001 (2013), dx.doi.org/10.1051/epjconf/20134011001.

71) P. Weiss and R. Forrer, Ann. Phys. **12**, 279 (1929).

72) A.L. Wysocki, R.F. Sabirianov, M. van Schilfgaarde, and K.D. Belashchenko, Phys. Rev. B **80**, 224423 (2009).

73) A. Alam and A. Mookerjee, Phys. Rev. B **72**, 214207 (2005).

74) Thermal Conductivity: Theory, Properties, and Applications, edited by Terry M. Tritt (Kluwer Academic, New York, 2004).

75) C. Y. Ho, M. W. Ackerman, K. Y. Wu, T. N. Havill, R. H. Bogaard, R. A. Matula, S. G. Oh, and H. M. James, J. of Phys. and Chem. Ref. Data **12**, 183 (1983)

Table 1. Calculated majority (UP) spin states density of states (total in the case of nonmagnetic $Ni_{0.8}Cr_{0.2}$ and $Ni_{0.33}Co_{0.33}Cr_{0.33}$), $N(E_F)$, and Fermi velocities, $\sqrt{\langle v_x^2 \rangle}$, experimental [28] residual resistivity, calculated electron mean free path, $\boldsymbol{l}$, experimental lattice parameter [29], calculated magnetic moments of each components (separated by a slash) and Curie temperatures, T_C, both experimental [29] and calculated, within GGA and LSDA approximation for the exchange-correlation energy, and calculated residual resistivity (both GGA and LSDA).

	Ni	$Ni_{0.5}Co_{0.5}$	$Ni_{0.5}Fe_{0.5}$	$Ni_{0.33}Co_{0.33}Fe_{0.33}$	$Ni_{0.8}Cr_{0.2}$	$Ni_{0.33}Co_{0.33}Cr_{0.33}$
$N(E_F)$ (UP), St./Hart.	4.3	2.0	4.0	3.0	45.13	44.05
$\sqrt{\langle v_x^2 \rangle}$ (UP), 10^6 m/s	0.43	0.46	0.46	0.46	0.24	0.24
Exp. ρ, μΩ·cm	0.1	2.07	10.37	4.87	77	93.21
l (UP), Å	3595	1689	174	478	4.1	4.0
a, Å	3.524	3.5345	3.5825	3.569	3.595	3.559
Magn. Mom., μ_B	0.56	0.62/1.64	0.63/2.54	0.63/1.57/2.42	—	—
Exp. T_C, K	628	1117	780	995	—	—
Calc. T_C (GGA/LDA), K	342/298	1180/990	955/810	1180/1045	—	—
Calc. ρ (GGA/LDA), μΩ·cm	-	0.7/0.9 [63]	2.1/3.3 [63]	1.9/2.9 [63]	78.1/77.0	68.6/67.6 [63]

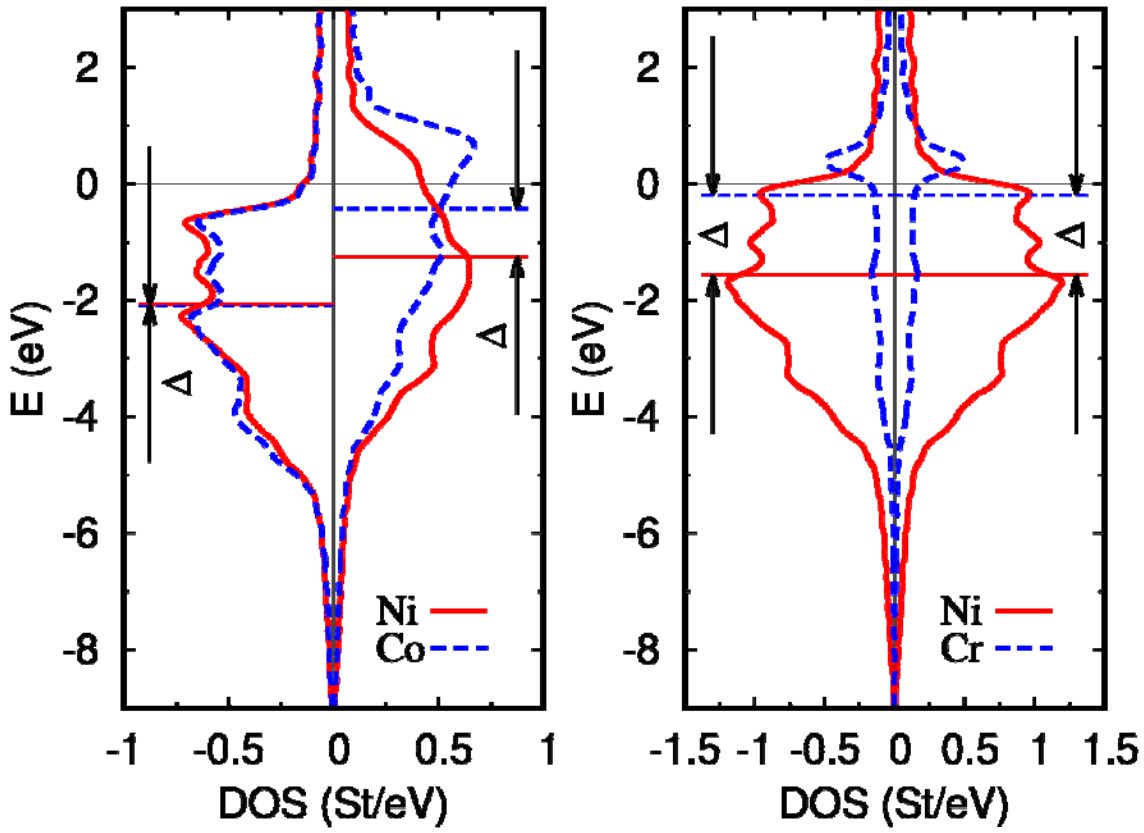

Figure 1. Projected density of states of magnetic NiCo (left) and nonmagnetic $Ni_{0.8}Cr_{0.2}$ (right) shown by dashed blue lines for Co/Cr and solid red line for Ni atoms. The Fermi energy corresponds to zero on the vertical axis. The centers of the *d*-bands are shown by horizontal lines, where splitting is denoted by Δ.

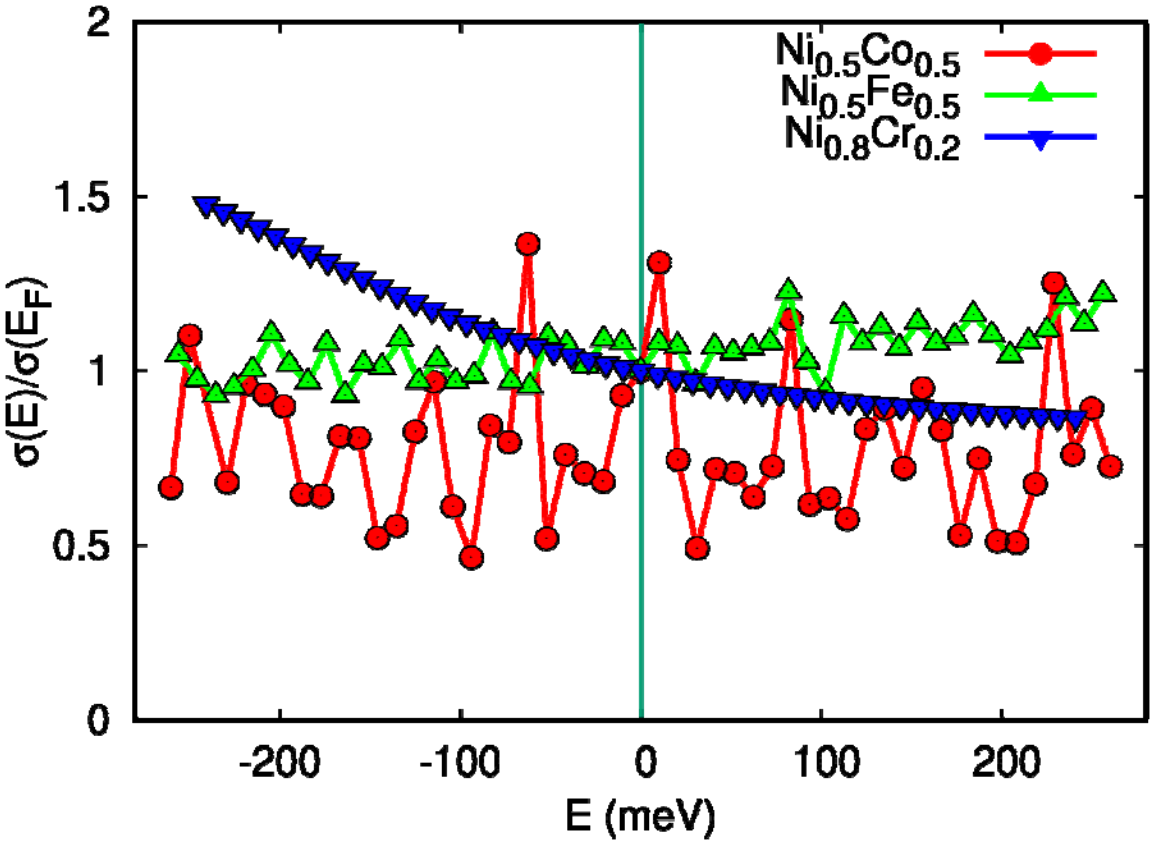

Figure 2. Static electrical conductivity as a function of energy calculated in three alloys. The Fermi energy corresponds to zero.

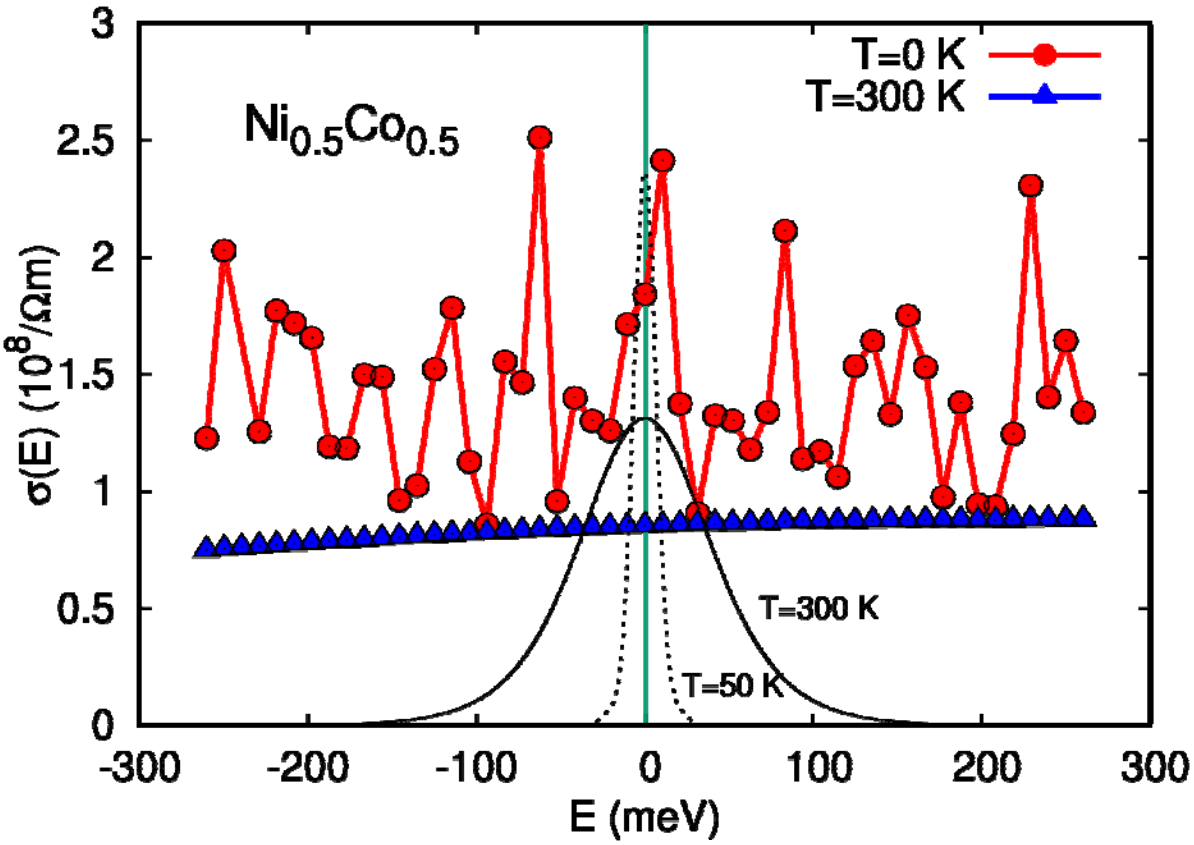

Figure 3. Electrical conductivity in $Ni_{0.5}Co_{0.5}$ as a function of energy calculated with magnetic moment fluctuation at temperature T=300 K (blue line with triangles) and with perfect magnetic ordering (red line with circles). The derivative of Fermi distribution function ($-\partial f/\partial E$) is shown by black solid (T=300 K) and dashed (T=50 K) lines in relative units.

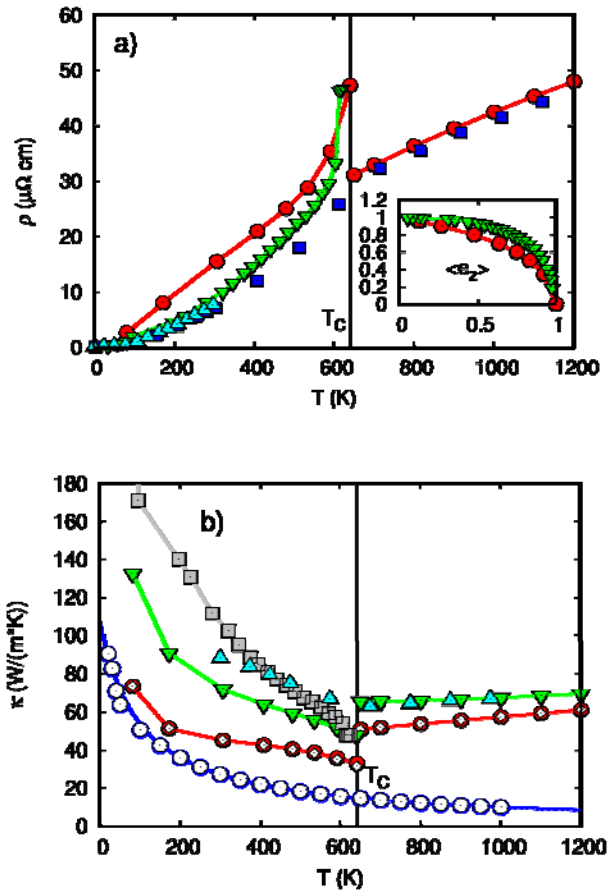

Figure 4. a) Electrical resistivity in Ni as a function of temperature calculated using CFM results for the magnetization (red line with filled circles) and experimental magnetization (green down triangles), the experimental resistivity is shown by upper triangles [28] and blue color filled squares [75]. Both experimental (green down triangles) and calculated (red circles) magnetization dependences of T/T_C, are shown in the insert. b) Thermal conductivity, κ, as a function of temperature calculated using Eq. (7) and theoretical results for magnetization (WF law result is shown by red line with filled circles, the result with correction to WF law is shown by empty diamonds). The lattice contribution to κ is shown as blue line with open circles. Total κ calculated using theoretical magnetization is shown as a green line with down triangles, whereas, calculated using experimental magnetization is shown as a grey line with filled squares, experiment [29] is shown as upper cyan triangles. The experimental T_C is indicated by a vertical line. All the calculated dependencies include scattering on both lattice vibrations and magnetic moment fluctuations.

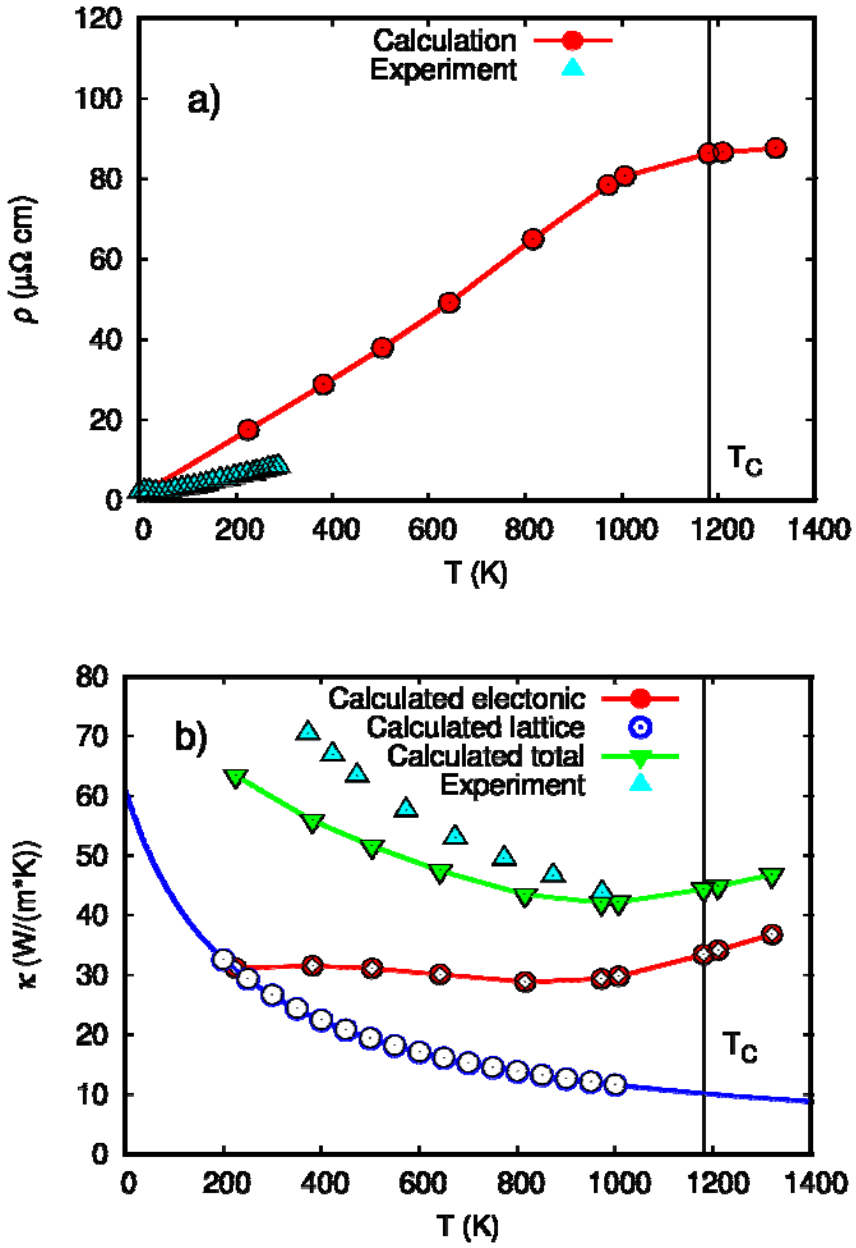

Figure 5. a) Electrical resistivity, and b) thermal conductivity in $Ni_{0.5}Co_{0.5}$. For notations see Fig. 4. In addition to the contribution from electrons scattering on lattice vibrations and magnetic moment fluctuations, the result presented by a red line with filled circles contains a contribution from scattering on "chemical" disorder. The calculated T_C is indicated by a vertical line.

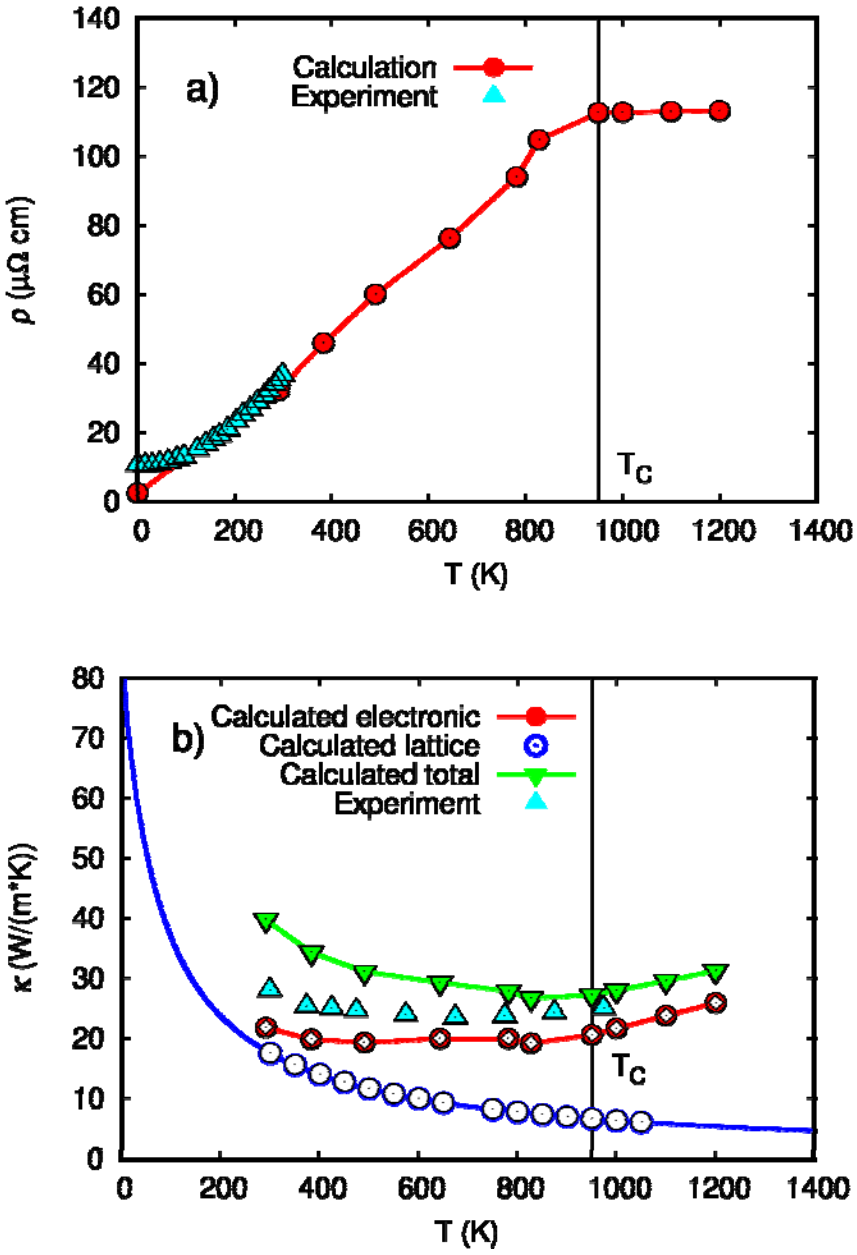

Figure 6. a) Electrical resistivity, and b) thermal conductivity in $Ni_{0.5}Fe_{0.5}$. For notations see Fig. 4. In addition to the contribution from electrons scattering on lattice vibrations and magnetic moment fluctuations, the result represented by a red line with filled circles contains a contribution from scattering on "chemical" disorder. The calculated T_C is indicated by a vertical line.

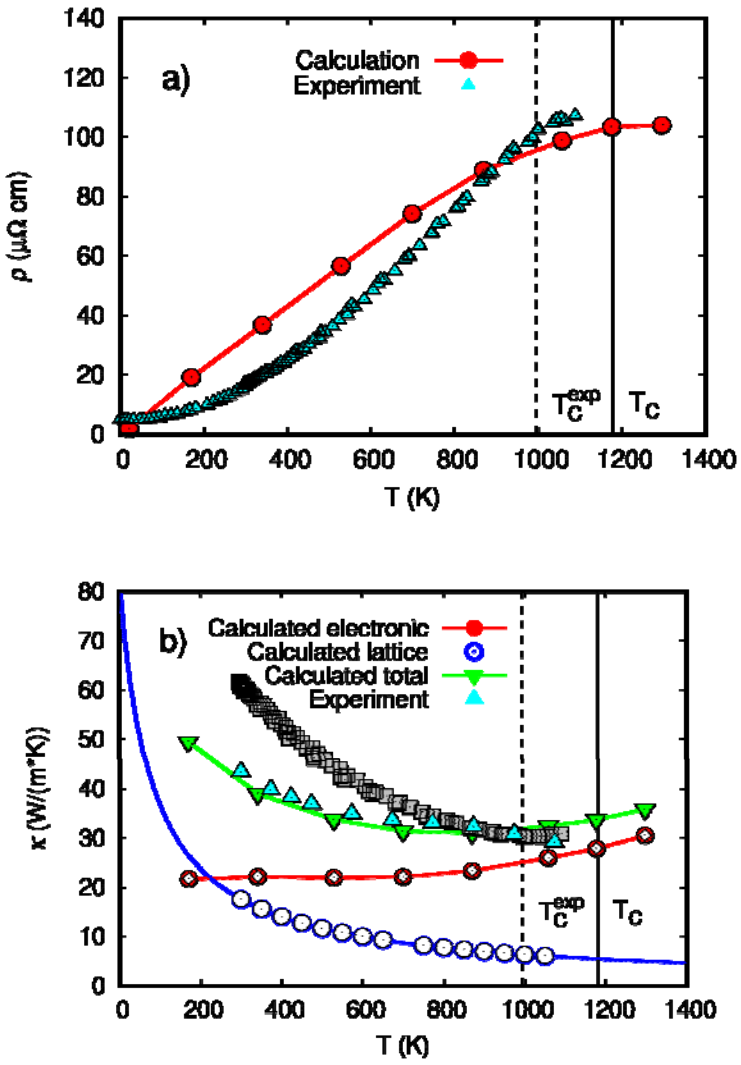

Figure 7. a) Electrical resistivity, and b) thermal conductivity in $Ni_{0.33}Co_{0.33}Fe_{0.33}$. For notations see Fig. 4. In addition to contribution from electrons scattering on lattice vibrations and magnetic moment fluctuations, the result represented by a red line with filled circles contains a contribution from scattering on "chemical" disorder. The total thermal conductivity calculated as a sum of lattice contribution and the electronic contribution obtained from experimental resistivity (cyan triangles in Fig. 7 (a)) through the WF law is shown by grey color squares. The calculated, T_C, and experimental, T_C^{exp}, Curie temperatures are indicated by solid and dashed vertical lines, respectively.

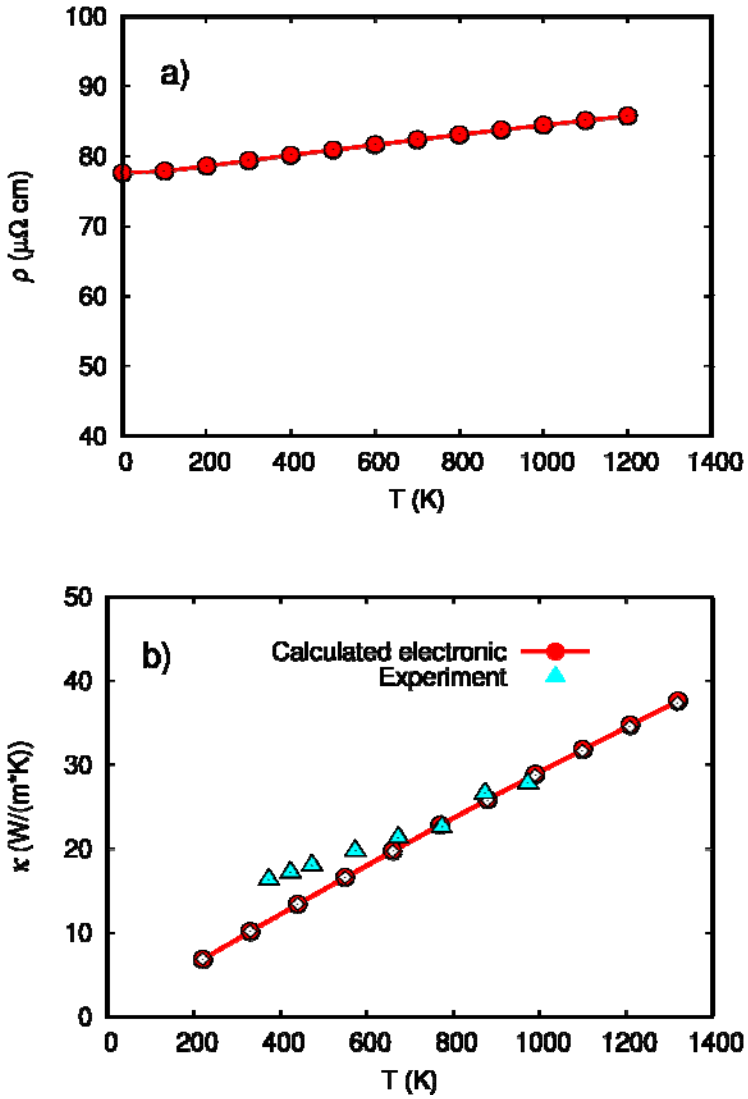

Figure 8. a) Electrical resistivity, and b) the electronic part of the thermal conductivity in $Ni_{0.8}Cr_{0.2}$. For notations see Fig. 4. The calculations have been done in the nonmagnetic state.

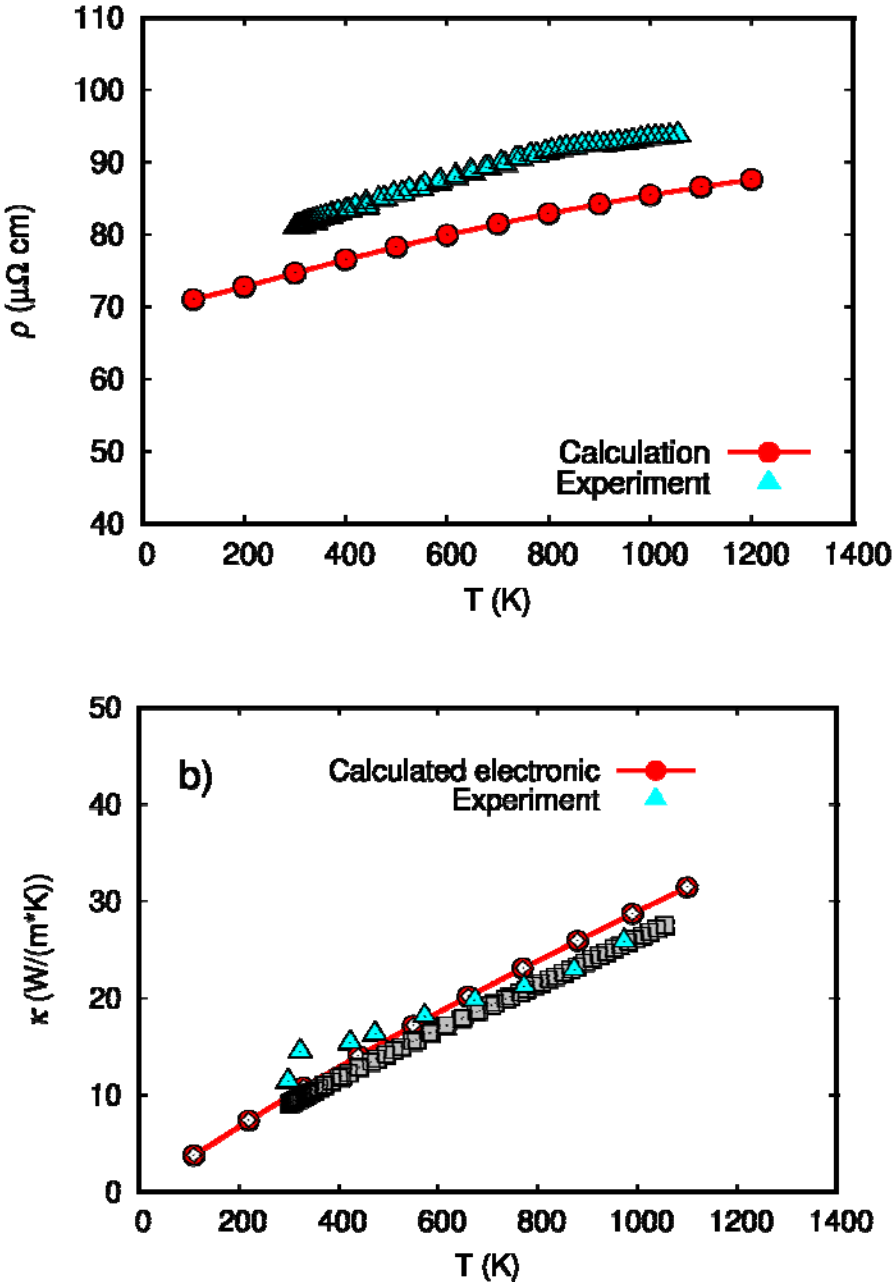

Figure 9. a) Electrical resistivity, and b) the electronic part of the thermal conductivity in $Ni_{0.33}Co_{0.33}Cr_{0.33}$. For notations see Fig. 4. The calculations have been done in the nonmagnetic state. The experimental resistivity obtained in the current work for the compound $Ni_{0.35}Co_{0.35}Cr_{0.3}$ is shown as cyan color triangles. The electronic part of the thermal conductivity calculated from the experimental resistivity (cyan triangles in Fig. 9 (a)) through the WF law is shown as grey color squares.